Porosity Analysis in Metal Additive Manufacturing by Micro-CT

S. Shrestha[1], K. Chou[1]

[1]University of Louisville, Additive Manufacturing Research Center, Vogt Bldg., Rm. 101, 100 Eastern Pkwy., Louisville, KY 40292, USA

Aims

This study aims at pore measurements and analysis for a laser powder-bed fusion additive manufacturing (AM) process, commonly known as selective laser melting (SLM). SLM utilizes a high-power laser, continuously moving, to heat and melt the powder particles and form a solid part. Due to its additive feature, very complex geometry can be fabricated, otherwise either impossible or difficult to make using conventional manufacturing. Porosity is one of the most problematic defects in SLM parts; it impairs the part performance, and yet, is sharply sensitive to the parameters of the SLM process itself. There are different mechanisms of pore formation in SLM, one being related to the keyhole phenomenon, caused by high energy density. Some studies have been carried out to understand the effect of energy density on keyhole pores by the means of metallography[1-2]. However, detailed analysis of SLM pore formations using a CT technique is desired in order to understand the severity of pore formations at different process conditions. Micro-CT has been applied to study the interior voids formed during SLM of aluminum alloy[3], cobalt-chrome[4], Ti-6Al-4V[5]. In this study, an SLM system was used to fabricate semi-hollow cylinder samples with single tracks formed inside with different process parameters. A micor-CT scanner was used to measure the internal geometry of the SLM specimens and to analyze the porosity in single tracks formed with different parameters.

Method

SLM specimen fabrications

Figure 1 shows EOS M270 used to fabricate SLM specimens for pore analysis in this study. At first, powder particles are spread above the build plate, then, the laser source scans the desired area line by line. After complete scanning of one layer, a successive layer is spread over and laser scanning is made, which is carried out until the final desired part is obtained. Ti-6Al-4V powder particles with the size below 45 µm were used and the layer thickness was 30 µm. Two levels of laser power (175 W and 195 W) and scanning speeds ranging from 200 mm/s to 1200 mm/s were tested

Figure 1: An EOS M270 SLM system used for specimen fabrications (left) and a photo showing SLM process (right).

To systematically and consistently access the build regions subject to CT measurements, a small cylinder-shape model of half-solid and half-hollow was designed. Figure 2 (a) shows the CAD model of a semi-hollow cylinder. The notches with end-to-end dimension of 12 mm were included to identify the start and end of single tracks. For one specimen, four single tracks can be formed, with specified process parameters, at the top of the base pad (half-solid cylinder). The specimens of such a model were then fabricated in M270; Figure 2(b) shows the specimens after the build completion.

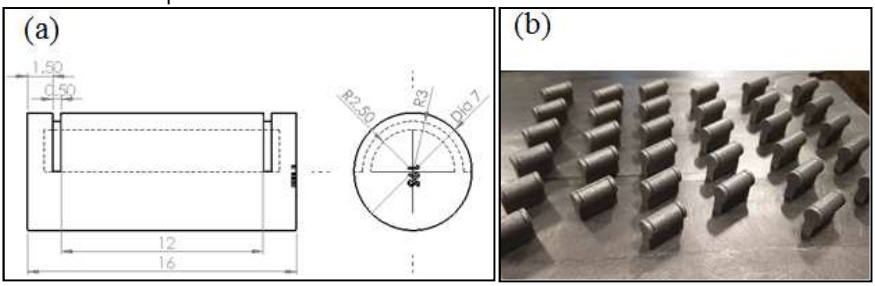

Figure 2: (a) CAD model of the specimen (unit in mm) and (b) Semi-hollow cylinders with single track built on the base plate.

CT scanning

CT scanning of the fabricated single-track SLM specimens was performed in a Bruker SkyScan 1173 micro-CT scanner. The test specimen was positioned in the brass sample mount using clay, styrofoam and parafilm tape as shown in Figure 3. A magnification of 6 µm was used and samples were scanned at 2000 resolution. 130 kV x-ray source with 8 W power was generated which is filtered through a 0.25 mm brass filter so to cut off x-ray with energy below 60 kV. Using 0.1° rotational angle to perform complete 360° scanning, each specimen required about 17.5 hours of scanning time. Due to long scanning time, flat field correction was performed every 60 minutes to minimize the effect of thermal movement. As a result, the reconstruction process did not require project pixel shift corrections. After scanning was completed, the steps towards reconstruction were followed. Beam hardening of 30% have been used which remained the same for all the samples. Ring artifacts and misalignment compensations were performed using parameter fine-tuning to minimize the ring artifacts and blurring effects, etc.

Figure 3: Specimen setup in the CT system showing near x-ray window (Left) and closed-up view (Right).

CTan software was used to analyze the reconstructed data. At first, top and bottom for the volume of interest were selected which defined the start and end of scanning track. Then, a

rectangular region of interest (ROI) was specified which was kept consistent for every track in all specimens. The region of 0.4 mm x 0.5 mm was selected and the position was changed based on the slice to exclude the powder area from the region of interest. Figure 4 below illustrates the region of the interest in reference to one single track. After the ROI was expanded to all slices, the binary images were obtained. Then, 3D morphometry analysis was performed to obtain the pore information such as the volume. Since the number of pores from each single track was limited, individual pore analysis has been conducted. The individual pore analysis help obtain the pore volume of any specific pore along with its location along the single track.

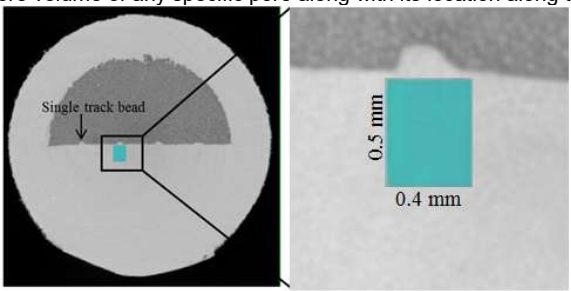

Figure 4: Selection of ROI beneath single track for porosity analysis.

Results

Typical scanning images

Figure 5 shows examples of CT images from one specimen with different sectional views as well as the isometric partial cutoff view. The light grey area is solid, the medium grey area is powder and the dark spots in the sagittal view are pores. These are the pores due to keyhole formation when the recoil pressure creates huge depression which was not filled before the solidification and the void were entrapped. In addition, Figure 6 shows the binary image of a pore at successive slices and the rendered 3D representation of a pore from the 2D information. Further, the 3D view of pores was generated from CTVox software by density cutoff which removes the highly dense Ti-6Al-4V solid from the view.

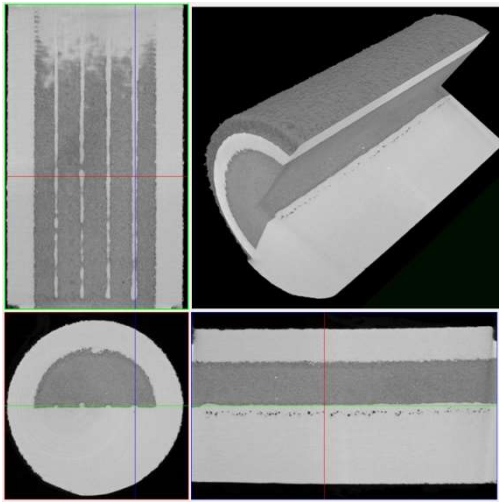

Figure 5: Examples of CT images of a scanned SLM specimen.

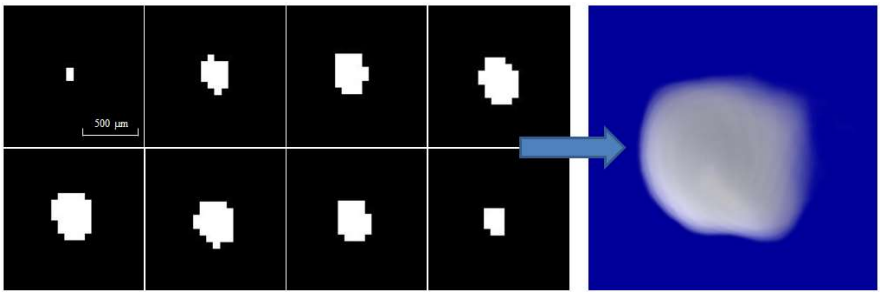

Figure 6: 3D rendering of a pore from 2D binary images.

Pore characteristics

To quantitatively characterize porosity, pore counts and individual volumes were obtained from CTan. For example, for 195 W power and 200 mm/s scanning speed, which has the maximum energy density (power over speed), the specimen exhibits 93 pores over the length of 12 mm. On the other hand, for the specimen with 195 W and 400 mm/s, Figure 7 shows the volume of each pore along the scanning direction. The pores are of varying size despite the same scanning speed through the entire scanning length.

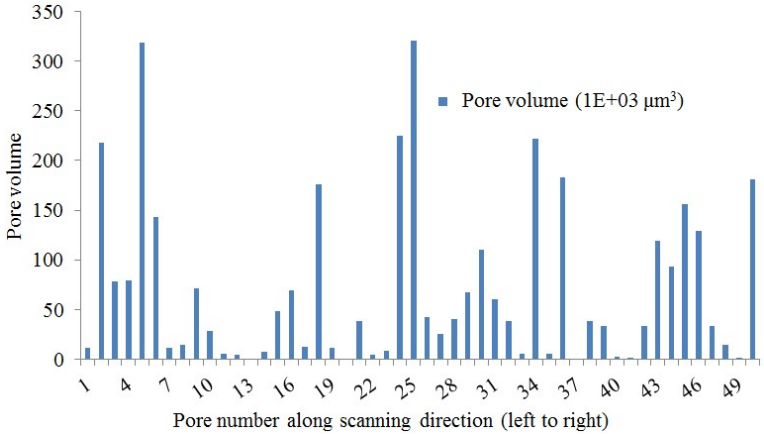

Figure 7: Pore volume along the scanning track of 195 W, 400 mm/s case.

Process parameter effects

The energy density during laser scanning, directly related to the laser power and scanning speed, plays a critical role of the keyhole phenomenon and associated pore formations. When the laser power is kept constant, decreasing the scanning speed increases the energy density, and therefore, promotes the formation of keyhole pores. As an example, Figure 8 compares between different speeds when the laser power is 195W. One may notice that for 200 mm/s scanning speed, a series of pores are formed which are well below the solid-powder interface. The keyhole effect is less noticeable for 600 mm/s, whereas the pore numbers decrease significantly for 1000 mm/s. Figure 9 shows the rendered 3D pore morphology observed at different scanning speed for 195 W laser power.

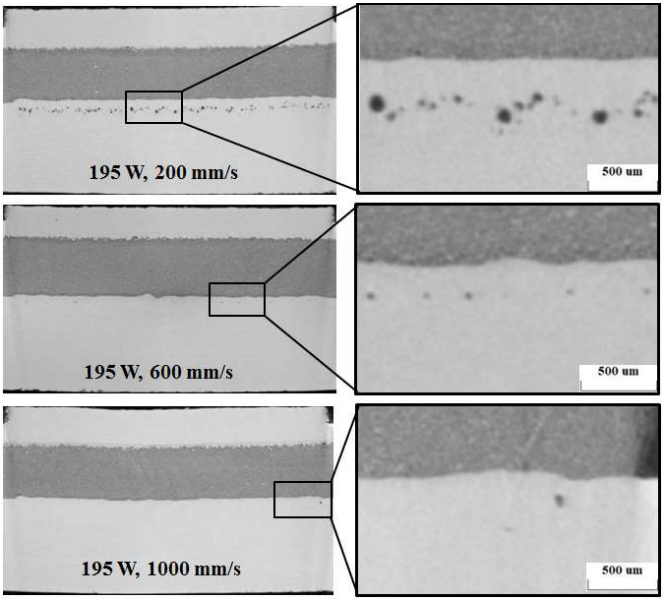

Figure 8: 2D images for pore comparisons between different scanning speeds.

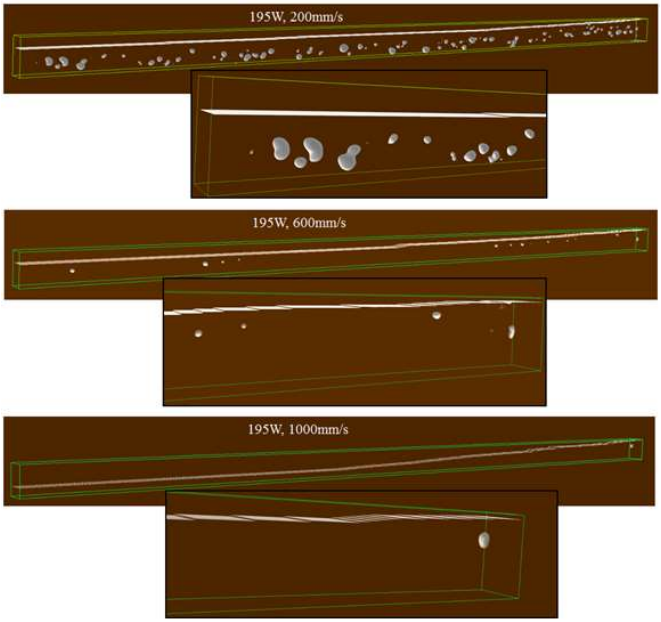

Figure 9: 3D view of pores from single tracks with different speeds.

Individual pore analysis was conducted and the detail information of pore counts and the total pore volume is summarized in Figure 10 for 2 levels of laser power and 6 different scanning speeds. The result shows that both the pore volume and the pore count reduce when the scanning speed increases, i.e., from a higher to lower energy density. The porosity seems to become insignificant when the scanning speed is above 600 mm/s.

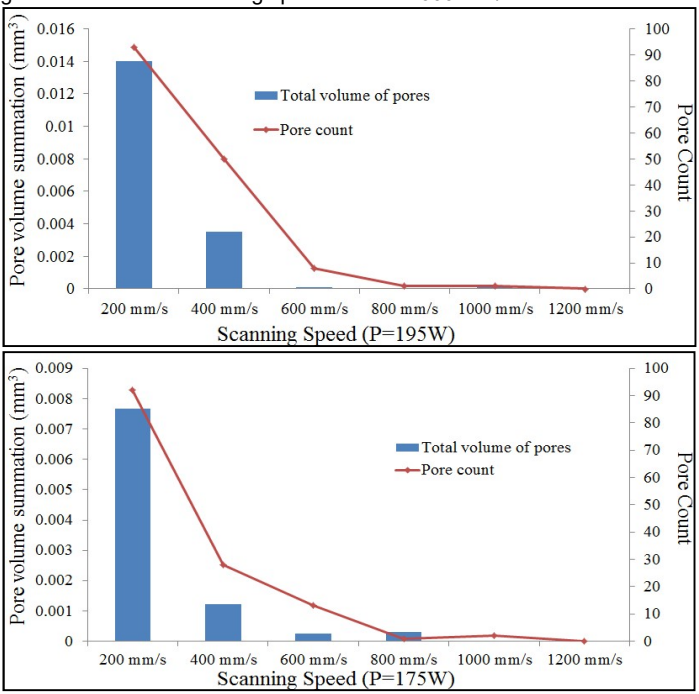

Figure 10: Pore population at different scanning speeds for 195 W (top) and 175 W (bottom).

Conclusion

Porosity analysis in SLM single-track specimens was performed using a SkyScan 1173 micro-CT scanner. The results clearly show pores resulted from the keyhole phenomenon in SLM and porosity reduction with the increased scanning speed because of a lower energy density. This study demonstrates the feasibility of using micro-CT for pore measurements and analysis in SLM. The methodology not only helps understand the pore shape, size, and population, etc., but also quantifies the process parameter effects on keyhole pore formations. Micro-CT offers a powerful tool to study the pore formations in metal AM such as SLM. Future work will extend this method to investigate pores created by different formation mechanisms and from different material powder and different metal AM processes.

References:

1. Gong, H., Gu, H., Zeng, K., Dilip, J., Pal, D., Stucker, B., Christiansen, D., Beuth, J., and Lewandowski, J. J., "Melt pool characterization for selective laser melting of Ti-6Al-4V pre-alloyed powder," Proc. Solid freeform fabrication symposium, pp. 256-267, 2014.

2. Dilip, J., Anam, M. A., Pal, D., and Stucker, B., "A short study on the fabrication of single track deposits in SLM and characterization," Proc. Solid freeform fabrication symposium, pp. 1644-1659, 2016.
3. Holesinger, T. G., Carpenter, J. S., Lienert, T. J., Patterson, B. M., Papin, P. A., Swenson, H., and Cordes, N. L., "Characterization of an aluminum alloy hemispherical shell fabricated via direct metal laser melting," JOM, 68(3), pp. 1000-1011, 2016.
4. Slotwinski, J. A., Garboczi, E. J., and Hebenstreit, K. M., "Porosity measurements and analysis for metal additive manufacturing process control," Journal of research of the National Institute of Standards and Technology, 119, p. 494, 2014.
5. Van Bael, S., Kerckhofs, G., Moesen, M., Pyka, G., Schrooten, J., and Kruth, J.-P., "Micro-CT-based improvement of geometrical and mechanical controllability of selective laser melted Ti6Al4V porous structures," Materials Science and Engineering: A, 528(24), pp. 7423-7431, 2011.

Acknowledgements
This study is supported by U.S. National Science Foundation under a grant (162662) from the Manufacturing Machine and Equipment program.